Heliyon 10 (2024) e23636

Contents lists available at ScienceDirect

Heliyon

journal homepage: www.cell.com/heliyon

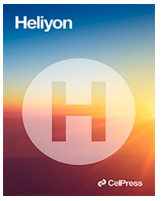

Construction of a diagnostic model for osteoarthritis based on transcriptomic immune-related genes

Bo Chen [a,1], Chun Lin [a,1], Xing Jin [a], Xibin Zhang [a], Kang Yang [a], Jianjian Wang [a], Feng Zhang [a], Yuxin Zhang [b,c], Yingying Ji [d], Zhaoxiang Meng [a,*]

[a] *Rehabilitation Medicine Department, Northern Jiangsu People's Hospital, Yangzhou, Jiangsu, 225001, China*
[b] *Department of Oral Surgery, Shanghai Ninth People's Hospital, Shanghai Jiao Tong University School of Medicine, College of Stomatology, Shanghai Jiao Tong University, National Center for Stomatology, National Clinical Research Center for Oral Diseases, Shanghai Key Laboratory of Stomatology, Shanghai 200011, China*
[c] *Department of Rehabilitation Medicine, Huangpu Branch, Shanghai Ninth People's Hospital, Shanghai Jiao Tong University School of Medicine, Shanghai 200011, China*
[d] *The affiliated Wuxi Mental Health Center of Jiangnan University, Wuxi Central Rehabilitation Hospital, Wuxi, Jiangsu, 214151, China*

ARTICLE INFO

Keywords:
Osteoarthritis
immune
Gene
Model
Biomarker

ABSTRACT

Background: Osteoarthritis (OA) is a leading cause of disability globally, affecting over 500 million individuals worldwide. However, accurate and early diagnosis of OA is challenging to achieve. Immune-related genes play an essential role in OA development. Therefore, the objective of this study was to develop a diagnostic model for OA based on immune-related genes identified in synovial membrane.

Methods: The gene expression profile of OA were downloaded based on four datasets. The significantly differentially expressed genes (DEGs) between OA and control groups were selected. The differential immune cells were analyzed, followed by immune-related DEGs screening. WGCNA was used to screen module genes and these genes were further selected through optimization algorithm. Then, nomogram model was constructed. Chemical drug small molecule related to OA was predicted. Finally, expression levels of several key genes were validated by qRT-PCR through construction of OA rat models.

Results: The total 656 DEGs were obtained. Eight immune cells were significantly differential between two groups, and 317 immune-related DEGs were obtained. WGCNA identified three modules. The genes in modules were significantly involved in 15 pathways, involving in 65 genes. Then 12 DEGs were screened as the final optimal combination of DEGs, such as *CEBPB*, *CXCL1*, *JUND*, GABARAPL2 and *PDGFC*. The Nomogram model was also constructed. Furthermore, the chemical small molecules, such as acetaminophen, aspirin, and caffeine were predicted. The expression levels of *CEBPB*, *CXCL1*, GABARAPL2 and *PDGFC* were validated in OA rat models.

Conclusion: A diagnostic model based on twelve immune related genes was constructed. These model genes, such as *CEBPB*, *CXCL1*, GABARAPL2, and *PDGFC*, may serve as diagnostic biomarkers and immunotherapeutic targets.

* Corresponding author. Rehabilitation Medicine Department, Northern Jiangsu People's Hospital, No. 98, Nantong West Road, Guangling District, Yangzhou, Jiangsu, 225001, China.
E-mail address: yzmzx001@163.com (Z. Meng).
[1] Co-first authors.

https://doi.org/10.1016/j.heliyon.2023.e23636
Received 11 August 2023; Received in revised form 8 December 2023; Accepted 8 December 2023
Available online 13 December 2023
2405-8440/© 2023 The Authors. Published by Elsevier Ltd. This is an open access article under the CC BY-NC-ND license (http://creativecommons.org/licenses/by-nc-nd/4.0/).

1. Introduction

Osteoarthritis (OA) is a prevalent joint disorder that is characterized by the degradation of cartilage, inflammation of the synovium, and remodeling of the subchondral bone, which processes ultimately result in the impairment of joint function [1,2]. The pathophysiology of OA is complex and involves multiple factors, including inflammation and fibrosis of the infrapatellar fat pad and meniscus degeneration [3,4]. OA is a leading cause of disability around the world [5], affecting more than 500 million people worldwide [6]. The major risk factors of OA include aging, female gender, obesity and joint injuries [7]. Therefore, timely diagnosis and effective treatment are crucial for OA patients. However, the conventional diagnosis of OA relies on clinical symptoms and joint imaging techniques that can only detect the structural changes in a late stage of the disease, when the tissue damage is irreversible. Moreover, the interpretation of imaging results is subjective and may vary among radiologists, leading to potential misdiagnosis. Thus, accurate and early diagnosis of OA is challenging to achieve [8]. Therefore, identifying biomarkers for early OA diagnosis is essential to improve patient prognosis.

It is evidenced that synovial membrane is a precursor of joint failure and synovitis plays an important etiopathogenical role in OA [9]. The infrapatellar fat pad, located adjacent to the synovial membrane, appears to function as an anatomo-functional unit with the synovial membrane in OA [10,11]. Recent discoveries have underscored the critical involvement of immunological mechanisms in the etiology of OA [12,13]. The inflammatory synovium is linked to increased pain and damage to cartilage and menisci [14–16]. Additionally, immune complexes and immunoglobulins against cartilage components have been detected in cartilage and synovium of patients with OA [17]. Recent studies have increasingly highlighted the crucial role of immune cell infiltration in the development of OA. For instance, Bonnet et al. [18] have reported that chronic synovitis is characterized by cellular infiltration mainly composed of lymphocytes and macrophages, whereas acute synovitis is primarily marked by neutrophils. Similarly, Moradi et al. [19] noted significant infiltration of immune cells, including $CD14^+$ macrophages, $CD4^+$ T cells, and $CD8^+$ T cells, within OA-afflicted joints. As a result, identification of immune system-related biomarkers may help develop novel diagnostic biomarkers and immunotherapeutic targets.

In this study, multiple microarray data on synovial membrane of OA were collected for analysis. The differentially expressed genes (DEGs) were screened and those related with immune were screened by combining with the immune evaluation of samples. Additionally, the optimized immune-related markers were screened by different optimization algorithms. Then, a nomogram diagnostic classification model was developed was constructed using the training dataset and verified using the another dataset. The key immune-related genes were further validated in an OA rat model by qRT-PCR. Finally, small molecular chemical drugs related to OA were predicted.

2. Methods

2.1. Screening of expression profile data

Fata retrieval was performed from Gene Expression Omnibus using the keywords "osteoarthritis" and "Homo sapiens". The following selection criteria for data retrieval were applied: 1) gene expression profile of human synovial membrane samples; 2) the samples were classified as normal controls and OA; 3) inclusion of at least 15 samples in the analysis. A total of 4 datasets (GSE55457, GSE55235, GSE12021 and GSE82107) meeting the screening criteria were obtained, The GEO datasets collected are exhibited in Table 1. Then, GSE55457, GSE55235, and GSE12021 were merged into a single gene expression matrix file, which served as the training dataset, while GSE82107 was used as the validation dataset. The dataset was batch normalized using the "sva" package version 3.38.0 of the R3.6.1 software [20].

2.2. Screening of significantly DEGs

In the training dataset, the R3.6.1 limma data (Version 3.34.7) package [21] was utilized to screen the significantly DEGs between OA and control groups. The thresholds for DEG screening were set as false discovery rate (FDR) < 0.05 and $|\log2 \text{ fold change}| > 0.5$. Then, the pheatmap package (version 1.0.8) [22] in R3.6.1 was employed to perform two-directional hierarchical clustering [23] for DEGss based on Euclidean distance [24].

2.3. Evaluation of immune cell types of samples

To assess the landscapes of immune infiltration in the training dataset, CIBERSORT [25] was employed to calculate the composition

Table 1
Table 1 Basic information of gene expression profiling.

Dataset	Platform	Tissue sample	Number of OA samples	Number of normal samples
GSE55457	GPL96	synovial membrane	10	10
GSE55235	GPL96	synovial membrane	10	10
GSE12021	GPL96	synovial membrane	10	9
GSE82107	GPL570	synovial membrane	10	7

proportions of 22 types immune cells based on the expression levels of the samples in the training dataset. Subsequently, the distribution differences of the immune cell proportions between the OA and control groups were compared using the Student t-test in R3.6.1.

2.4. Screening of DEGs associated with important immune cells

The correlation between the DEGs and the immune cell types with significant differences was evaluated using the Pearson correlation coefficient (PCC) calculated with the cor function in R version 3.6.1. DEGs with $|PCC| > 0.5$ were selected as immune-related DEGs. Subsequently, these underwent gene ontology biological process (BP) and KEGG pathway enrichment analyses using DAVID version 6.8 [26,27]. FDR <0.05 was selected as the threshold for enrichment significance.

2.5. Construction of protein–protein interaction (PPI) network and analysis of network topology

Protein interaction relationships among the immune-related DEGs were obtained by searching STRING 11.0 [28]. Subsequently, the PPI network was constructed using Cytoscape 3.9.0 [29]. To evaluate the centrality of the DEGs within the PPI network, three algorithms (betweenness centrality (BC), closeness centrality (CC), and degree centrality (DC)) were applied using the CentiScaPe plugin in Cytoscape [30].

2.6. Screening of modules associated with disease status and immune cell

The WGCNA package version 1.61 [31] in R3.6.1 was utilized to discern modules, which displayed noteworthy correlations with the clinical characteristics, encompassing diverse disease statuses and distinct immune cell infiltrations, based on the expression levels of all genes in the training dataset. The module division thresholds were set as follows: a module set needed to contain a minimum of 150 genes, and a cutHeight of 0.995.

Next, the immune-related DEGs were mapped to the modules that were associated with the clinical traits, and the fold enrichment and p-values were calculated using the Fisher exact test. The module screening thresholds were defined as $p < 0.05$ and fold enrichment >1. Subsequently, KEGG signaling pathway enrichment analysis based on DAVID version 6.8 [31] was conducted on the DEGs that showed significant enrichment within the module. The genes that demonstrated significant involvement in the relevant KEGG signaling pathway were selected for further analysis.

2.7. Important immune-related marker screening through optimization algorithm

In the training dataset, three optimization algorithms were employed for the selection of feature genes: random forest (RF), recursive feature elimination (RFE), and least absolute shrinkage and selection operator (LASSO). The performance of the RFE model was assessed by comparing the average misjudgment rates obtained from its 100-fold cross-validations, utilizing the "caret" software package [32]. RFE is a novel machine learning technique that recursively ranks features to prevent overfitting.

LASSO regression, on the other hand, is a dimension reduction approach that outperforms regression analysis when dealing with high-dimensional data. It utilizes regularization to improve prediction accuracy. In our study, LASSO regression was implemented using the "lars" package in R [33] to identify the gene signatures associated with the optimal lambda, resulting in the lowest classification error.

Lastly, RF is a supervised machine learning algorithm that utilizes a decision tree algorithm and is commonly used for regression and classification tasks. In our analysis, RF was performed using the "randomForest" package in R [34]. The importance of each feature was determined using the Mean Decrease Gini Index, calculated by RF.

2.8. Nomogram diagnostic model construction and validation

A Nomogram model was built using RMS package version 5.1-2 [35] based on the regression coefficient of each gene in R3.6.1. Then, based on the screened feature immune-related DEGs, decision curve analysis was performed on each DEG and the multi-DEGs combination model respectively using R3.6.1 RMDA package version 1.6 [36]. Finally, the efficacy of the diagnostic model was verified by constructing a Nomogram model in the GSE82107 validation dataset.

2.9. Animal models

Ten 6-week-old female Wistar rats (weighing 180–200 g), which were specific pathogen-free, were obtained from Shanghai SLAC Laboratory Animal Co. Ltd. (Shanghai, China). These rats, free from specific pathogens, were provided a period of one week to adapt to the standardized conditions of their housing prior to the commencement of the experiment. Rats were randomly assigned into model and control groups ($n = 5$ in each group). The left and right hind limbs of the rats were designated as the self-control, with the left side serving as the control side and the right side as the experimental side. The rats in model group were administered intraperitoneal anesthesia with 2 % pentobarbital sodium and positioned laterally for fixation. The knee was disinfected, toweled, and a 4 cm longitudinal skin incision was made. The subcutaneous tissues were then sequentially incised, followed by a lateral opening of the knee capsule. The anterior cruciate ligament was severed, and subsequently, the muscles, fascia, and skin were sutured in sequence.

Postoperative antibiotics were administered, with intramuscular penicillin (30,000 U per dose) given once daily for a duration of 3 days.

The rats were allowed to maintain their mobility on the operated side, and were closely observed for postoperative feeding and drinking, changes in hair color, incision healing status, suture detachment and infection. After 10 weeks, the synovial tissues were taken and stored at −80 °C.

2.10. qRT-PCR assay

The expression levels of *CEBPB*, *CXCL1*, *JUND*, GABARAPL2, and *PDGFC* in synovial tissues were detected by qRT-PCR. Total RNA was extracted from the tissues using RNAiso Plus (TAKARA, China), and the purity and concentration of the RNA were determined using a NanoDrop ND-1000 UV–vis spectrophotometer (Thermo Fisher Scientific). Subsequently, cDNA was synthesized from 1 μg of RNA using the PrimeScript™RT Master Mix (Perfect Real Time) (TaKaRa, China). For the qRT-PCR analysis, a final volume of 20 μL was used with Power SYBR Green PCR Master Mix (Thermo, USA). The amplification protocol consisted of an initial denaturation step at 95 °C for 10 min, followed by 40 cycles of denaturation at 95 °C for 15 s, annealing at 60 °C for 60 s, and a melting step at 95 °C for 15 s, 60 °C for 60 s, and 95 °C for 15 s. The primer sequences used for PCR are provided in Table 2.

2.11. Screening of small molecular chemical drug related to feature immune DEGs

All gene-chemicals connections were downloaded from the Comparative Toxicogenomics Database 2022 update (Davis et al., 2021). Then "osteoarthrisits" was used as the keyword to search chemical small molecule directly associated with OA disease in the CTD database. Subsequently, small chemical molecules that were linked to the feature immunity genes were extracted from all gene-chemical relationships and selected to be directly associated with OA, thus obtaining small chemical molecules associated with the feature immunity genes.

2.12. Statistical analysis

Statistical analysis was performed using 3.6.1 and Graphpad prism 5. The thresholds for screening DEGs were set at FDR <0.05 and $|\log2 \text{ fold change}| > 0.5$. The correlation between immune cells and the DEGs were analyzed by calculating the PCC. The immune-related DEGs were identified by retaining the ones with $|PCC| > 0.5$. The immune-related modules were screened based on $p < 0.05$ and fold enrichment >1. The differences between the two groups were calculated using Student's t-test, and a significance level of $P < 0.05$ was used as the screening criterion for determining significant differences.

3. Results

3.1. Identification of OA-related DEGs

Three datasets (GSE55457, GSE55235 and GSE12021) were combined into a training dataset by removing batch effects by sva algorithm. Fig. 1A clearly illustrates that prior to batch effect removal, the three datasets were obviously distributed in different areas. Fig. 1A clearly illustrates that prior to batch effect removal, the three datasets were visibly segregated in distinct regions. Conversely, after the application of batch effect correction, the samples from the three batches became intermingled (Fig. 1B), indicating successful elimination of the batch effect.

A total of 656 DEGs were identified from the training dataset. Among these genes, 317 were found to be down-regulated, while 339 were up-regulated in the OA group compared to the control group (Fig. 1C). Two-directional hierarchical clustering heatmap showed that the expression values of DEGs can successfully separate different types of samples, suggesting the robustness of DEGs (Fig. 1D).

Table 2
The primers used for PCR.

Primer	Sequence (5′-3′)
GAPDH-rF	AGACAGCCGCATCTTCTTGT
GAPDH-rR	CTTGCCGTGGGTAGAGTCAT
CEBPB-rF	GAGCTGACGGCGGAGAACGA
CEBPB-rR	GCATCAAGTCCCGAAACCC
CXCL1-rF	GCACCCAAACCGAAGTCA
CXCL1-rR	AAGCCAGCGTTCACCAGA
JUND-rF	GCATCGCCGCTTCCAAAT
JUND-rR	GACGCCAGCTCGGTGTTCT
GABARAPL2-rF	TAAAGTGACAAGGAGGGA
GABARAPL2-rR	AAAGTGGTAGAAGCGAGA
PDGFC-rF	GCGACAAGGAGCAGAACG
PDGFC-rR	GGCACAGTCCCAGAACCA

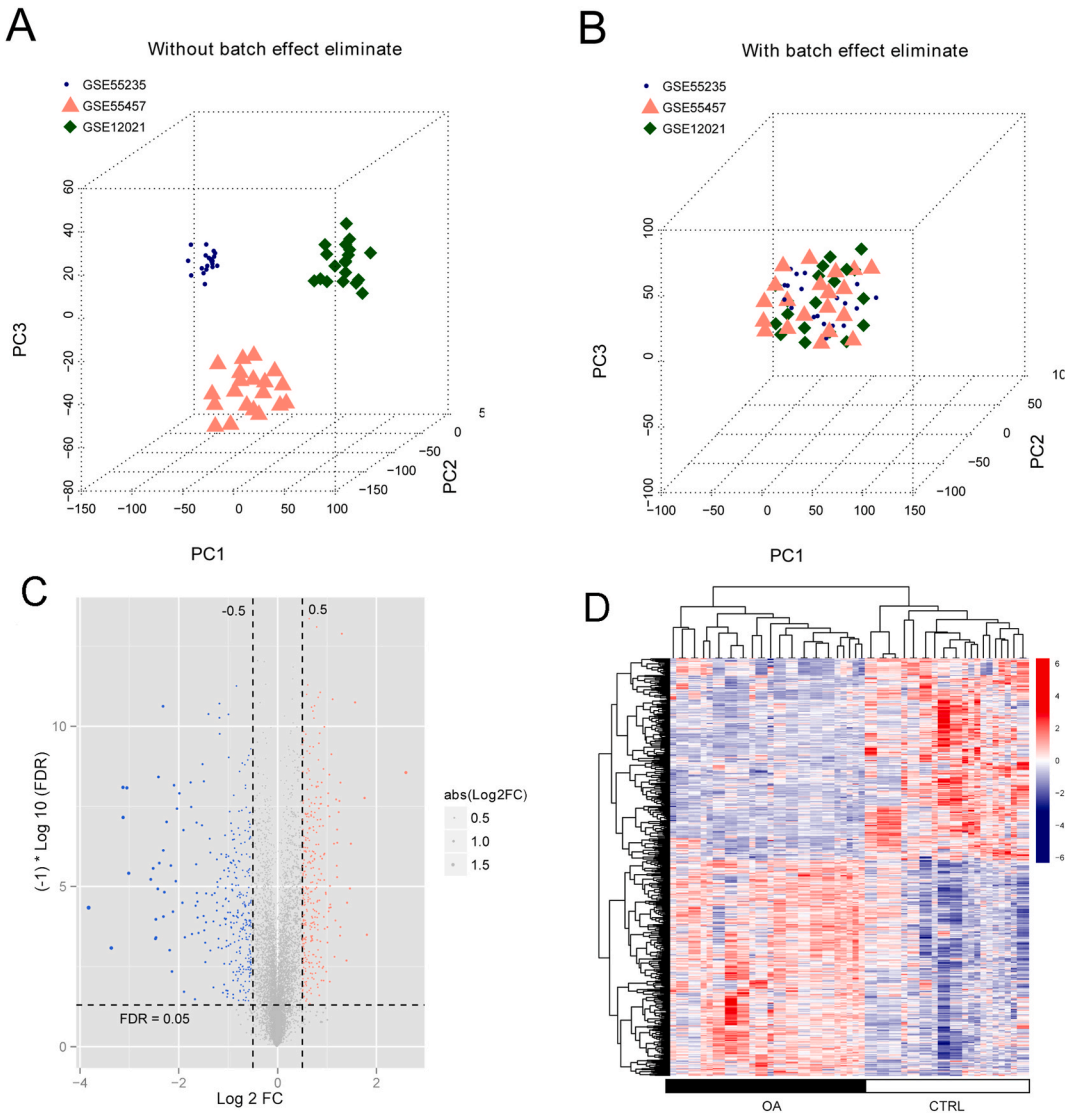

Fig. 1. Screening of significantly differentially expressed genes (DEGs). A and B: The sample relationships before (A) and after (B)batch effect removal, respectively. C and D: The (C) volcano map and (D) heatmap of DEGs. The blue and red dots in the volcano map indicate significantly downregulated and upregulated genes, respectively. (For interpretation of the references to color in this figure legend, the reader is referred to the Web version of this article.)

3.2. Screening of immune-related DEGs

The proportions of 22 immune cell types in OA and control samples were obtained by CIBERSORT (Fig. 2A). Significant differences were observed in the proportions of 8 immune cell types between the OA and control groups, including B cell memory, T cell regulatory (Tregs), T cell CD4$^+$ memory resting, eosinophil, mast cell resting, T cell CD4$^+$ naive, mast cell activated, as well as NK cell activated (Fig. 2B).

The PCCs between DEGs and the 8 immune cells were calculated and 317 immne-related DEGs were obtained (Fig. 3A). The functional enrichment analysis revealed that these DEGs were primarily enriched in several BP terms of “negative regulation of cell proliferation”, “cellular response to tumor necrosis factor”, and “inflammatory response”, as well as the KEGG pathways of “MPAK signaling pathway”, “TNF signaling pathway”, and “osteoclast differentiation” (Fig. 3B).

3.3. Construction of PPI network

The PPI relationships between 317 DEGs were searched in STRING, and relation pairs with an interaction score higher than 0.4 were retained. The PPI network contained 282 gene nodes and and 127 interaction pairs (Fig. 4).

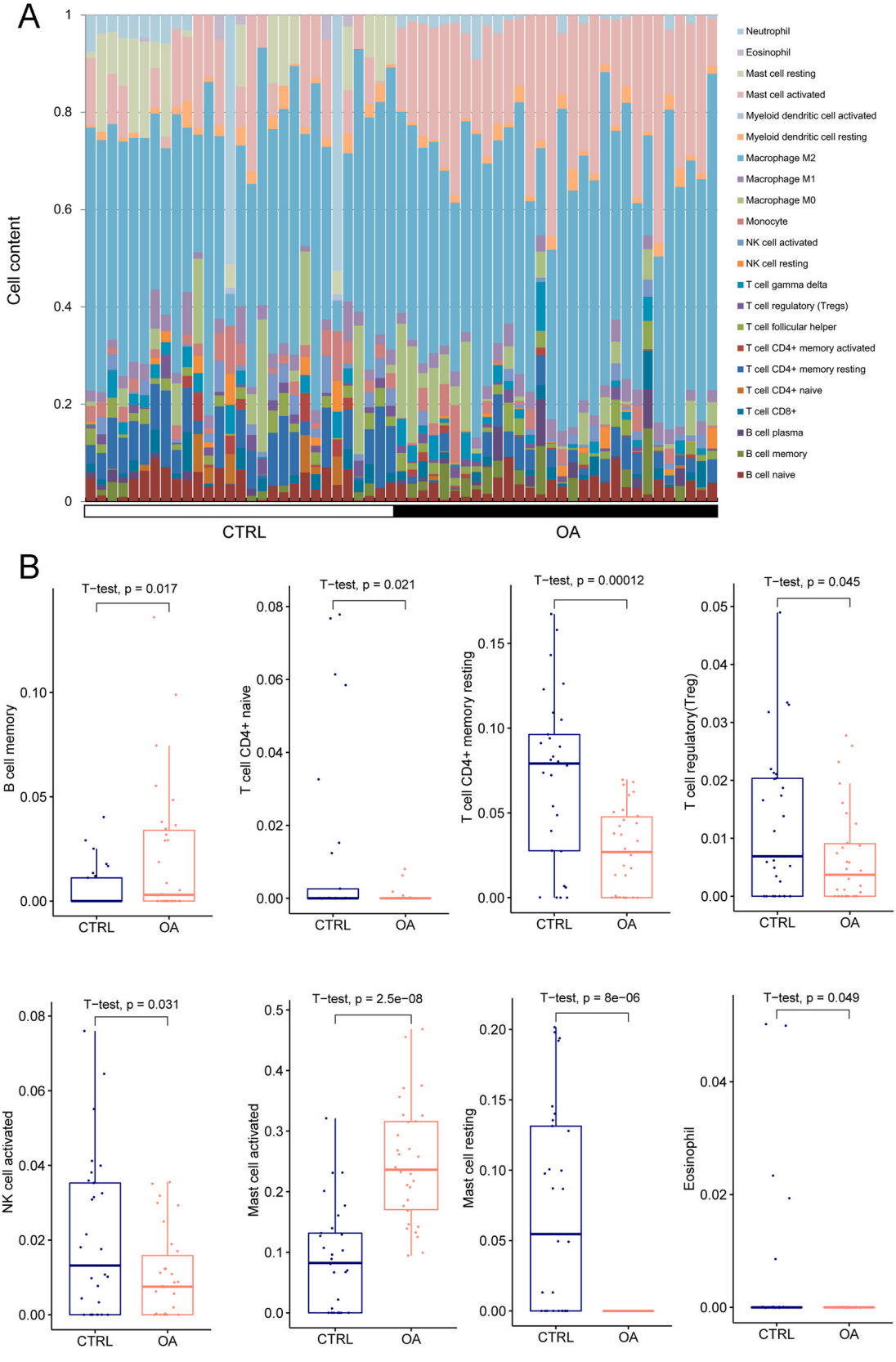

(caption on next page)

Fig. 2. Percentage of immune cells. A: The composition distribution of each immune cell in each sample. B: Eight immune cells were significantly differential between OA and control groups.

3.4. Screening of modules related to disease progression and immunity

The power value was determined at the point where the square of the correlation coefficient initially surpassed 0.9, and it was represented as power = 7. At this point, the co-expression network's average node connection degree was 1, aligning perfectly with the characteristics of a small-world network (Fig. 5A). Subsequently, the dissimilarity coefficient between nodes was computed, leading to the generation of a system clustering tree. By setting the minimum number of genes in each module to 150 and utilizing a cutHeight of 0.995 (Fig. 5B), ten modules were identified. Following this, a Multidimensional Scaling analysis was performed on the genes, revealing that genes contained in different modules exhibited a tendency to be distributed in the specific regions (Fig. 5C). The correlation between 8 important immune cells and each module is shown in Fig. 5D. The MEblue, MEred, Meyellow were highly correlated with the differential immune cells and disease status. Besides, MEturquoise, MEgreen, MEpink and MEbrown were also highly associated with the differential immune cells.

Then, the 317 immune-related DEGs were assigned to ten modules, and the analysis unveiled a significant enrichment of these immune-related DEGs within the MEblue, MEred, and MEturquoise modules, housing 112, 63, and 97 immune-related DEGs, respectively (Table 3). These Sixty-five genes were significantly involved in 15 pathways, including "MAPK signaling pathway", "IL-17 signaling pathway", "TNF signaling pathway", and "FoxO signaling pathway" (Table 4).

3.5. Screening of important immune-related markers

To identify the optimal combination of DEGs, three algorithms, namely LASSO, RFE, and RF, were employed based on the expression levels of 65 DEGs that were involved in significantly correlated pathways. The parameter diagram of the algorithm screening process is presented in Fig. 6A–C. Through the application of LASSO, RFE, and RF algorithms, 21, 20, and 30 DEGs were respectively selected. By comparing the results from these three sets of DEGs, 12 overlapping DEGs were identified. These 12 DEGs were determined as the final optimal combination for further analysis, including *CEBPB*, *CXCL1*, *DDX5*, GABARAPL1, GABARAPL2, JUND, *NDUFB5*, *NFKB2*, *NFKBIA*, *NR4A1*, *PDGFC*, and *UQCR10*.

3.6. Construction and verification of nomogram diagnostic model

According to the 12 immune DEGs factors, we utilized rmda package to analyze the decision curves for both individual DEGs and the combination model of multiple DEGs, and observed the net return rate of each DEG factor in relation to the diagnostic outcomes of the samples. Then, a nomogram was visualized by integrating the C-index values of the 12 immune-related DEGs in the training datasets of GSE55457, GSE55235 and GSE12021 (Fig. 6D). The disease stage can be predicted by calculating the total points obtained by adding the points of each gene. The calibration curves in Fig. 6E showed a strong agreement between the predicted probability and the actual outcome. Furthermore, we developed a nomogram model using the 12 immune-related DEGs in the validation dataset GSE82107, as illustrated in Fig. 6F. The calibration curves in Fig. 6G further confirmed the reliable performance of the nomogram in predicting the disease stage of OA. These findings indicate that the nomogram is robust across different datasets and holds promise as a valuable tool for disease stage prediction in OA.

3.7. Validation the expression level of key genes

The expression levels of 12 genes in both the training dataset and GSE82107 validation dataset were visualized (Fig. 7A and B). The findings revealed a remarkable concordance between the expression patterns of these 12 genes in the GSE82107 validation dataset, and the differential expression observed in the training dataset. In the GSE82107 validation dataset, the expression distribution of *CEBPB*, *CXCL1*, *DDX5*, GABARAPL1, GABARAPL2, *JUND*, *NDUFB5* and *PDGFC* exhibited significantly different between the OA and control groups ($P < 0.05$).

In addition, we selected five key genes that involved in inflammation related pathways, such as "NOD-like receptor signaling pathway" (GABARAPL2 and CXCL1), "TNF signaling pathway" (CEBPB and CXCL1), "IL-17 signaling pathway" (CEBPB, CXCL1 and JUND), "MAPK signaling pathway" (JUND and PDGFC), "NF-kappa B signaling pathway" (CXCL1), "FoxO signaling pathway" (GABARAPL2) and OA related pathway of "Osteoclast differentiation" (JUND) to be validated in an OA rat model. As shown in Fig. 7C, *CEBPB* and *CXCL1* were significantly lower in the OA group compared to the control group ($P < 0.05$). In the OA group, the expression levels of GABARAPL2 and PDGFC were found to be significantly upregulated compared to the control group ($P < 0.05$). However, no significant difference in JUND expression was observed between the two groups ($P > 0.05$).

3.8. Screening of small chemical molecules associated with feature immune DEGs

By integrating with the information of small molecular chemical drugs that were linked to 12 feature immune-related DEGs, 109 pairs of 12 feature gene-OA small molecular chemical drug interactions were obtained, involving 28 small molecular chemical drugs, such as acetaminophen, aspirin, caffeine, capsaicin, celecoxib, curcumin, diclofenac, dietary fats, and ethanol (Fig. 8 and Table S1).

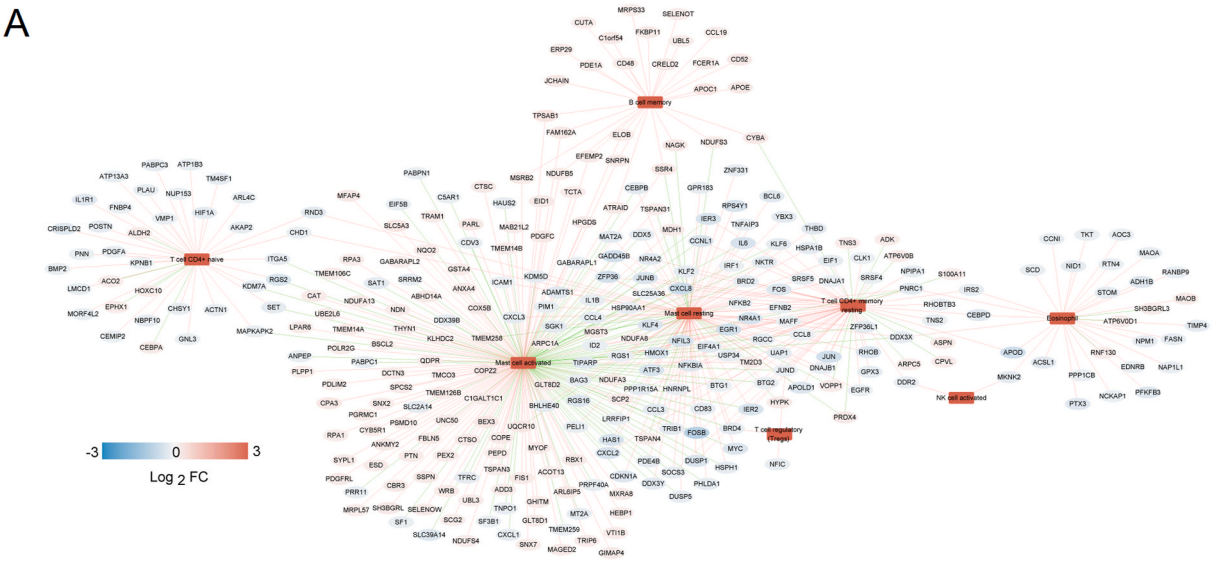

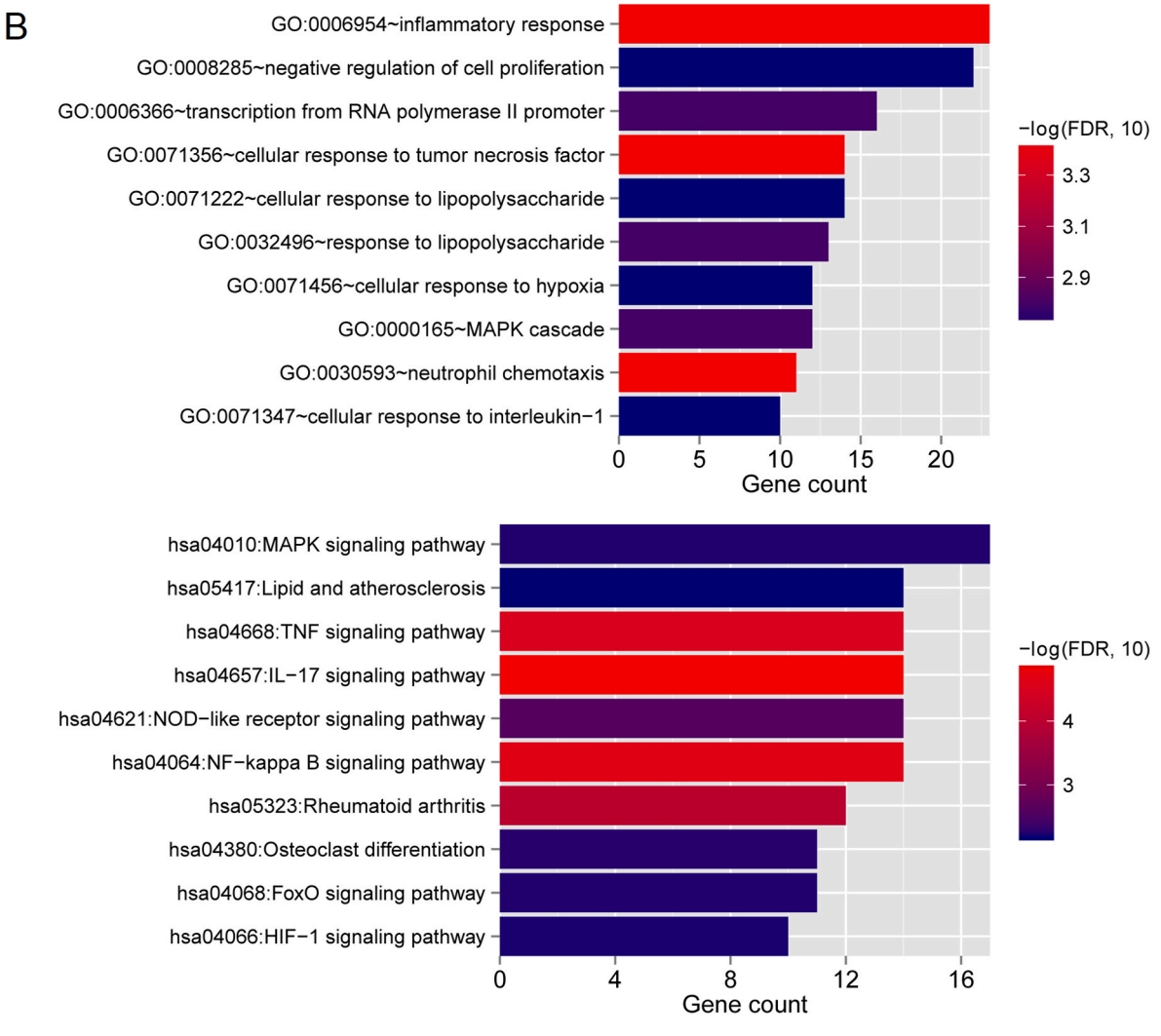

(caption on next page)

Fig. 3. Screening of DEGs significantly associated with important immune cells. A: Network diagram of immune cells and DEGs. Circles indicate DEGs and colors indicate degree of difference; Red squares indicate eight immune cell types. B: GO functions and KEGG signaling pathways enriched by immune-related genes. (For interpretation of the references to color in this figure legend, the reader is referred to the Web version of this article.)

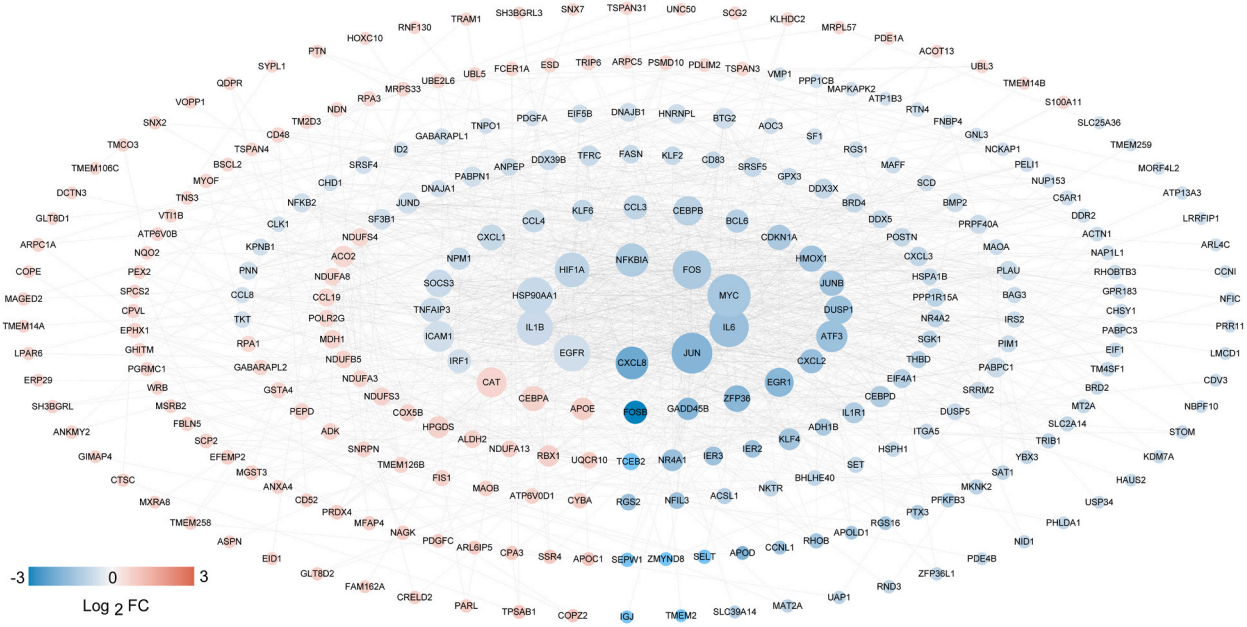

Fig. 4. The constructed interaction network. The color indicates the degree of significant difference and the size of the node indicates the degree of connectivity. (For interpretation of the references to color in this figure legend, the reader is referred to the Web version of this article.)

From Table S1, acetaminophen could affect the expression of CEBPB, DDX5, GABARAPL1 and NFKBIA, increase the expression of CXCL1, GABARAPL2, JUND, NFKB2 and NR4A1, and decrease the expression of NDUFB5 and PDGFC. Aspirin could promote the reaction of CEBPB binding to IL4 promoter polymorphism, increase the secretion of CXCL1, increase the expression of DDX5 and NFKBIA, and decrease the expression of JUND. Caffeine could decrease the expression of CEBPB and NDUFB5 and increase phosphorylation of NFKBIA.

4. Discussion

In this study, 317 immune-related DEGs were obtained, which were significantly enriched in various inflammation and immune-associated functions as well as pathways. After WGCNA, 65 genes were further selected. Then, based on LASSO, RFE and RF algorithms, 12 overlapping DEGs were finally screened out as the optimal combination, such as including *CEBPB*, *CXCL1*, *DDX5*, and GABARAPL1. Among these DEGs, the expression levels of 8 genes including *CEBPB*, *CXCL1*, *DDX5*, GABARAPL1, GABARAPL2, *JUND*, *NDUFB5* and *PDGFC* were comfirmed in the GSE82107 validation dataset. The qRT-PCR was used to validate the expression levels of *CEBPB*, *CXCL1*, GABARAPL2, and *PDGFC*. Furthermore, the small molecular chemical drugs, such as acetaminophen, aspirin, and caffeine were predicted.

A recent investigation has elucidated that OA is undergoing a transformative shift, evolving from a purely mechanical ailment attributed to cartilage degradation, to a multifaceted biological phenomenon that intertwines inflammation, biomechanics, and the immune system [37]. Therefore, we focused on immune-related genes in the present study by combining with immune evaluation of the samples. Significantly differential proportions of eight immune cell types were identified between the OA and control groups, including T cell $CD4^+$ memory resting, mast cell activated, T cell $CD4^+$ naïve, B cell memory, as well as mast cell resting. OA-affected joints have displayed a discernible pattern characterized by the infiltration of $CD4^+$ T cells. These $CD4^+$ T cells have the capacity to facilitate the polarization of activated Th1 cells and augment the secretion of cytokines, thereby exacerbating the progression of osteoarthritis [38]. Additionally, B cell infiltration was also reported in the synovial tissues of OA patients, with the extent of infiltration being directly correlated with the severity of local inflammation [39]. Mast cells are sentinels of the innate immune system, responding quickly to endogenous danger signals and exogenous pathogens [40]. It has been reported that the number and degranulation status of synovial mast cells are positively correlated with increased cartilage damage in patients with knee OA [41]. Taken together, our study further demonstrated the critical roles of immune cells in the pathogenesis of OA.

A nomogram consisting of 12 immune-related DEGs were developed to predict the disease stage of OA in this study. The calibration curves exhibited a robust concordance between the predicted probabilities and the observed outcomes in both the training and

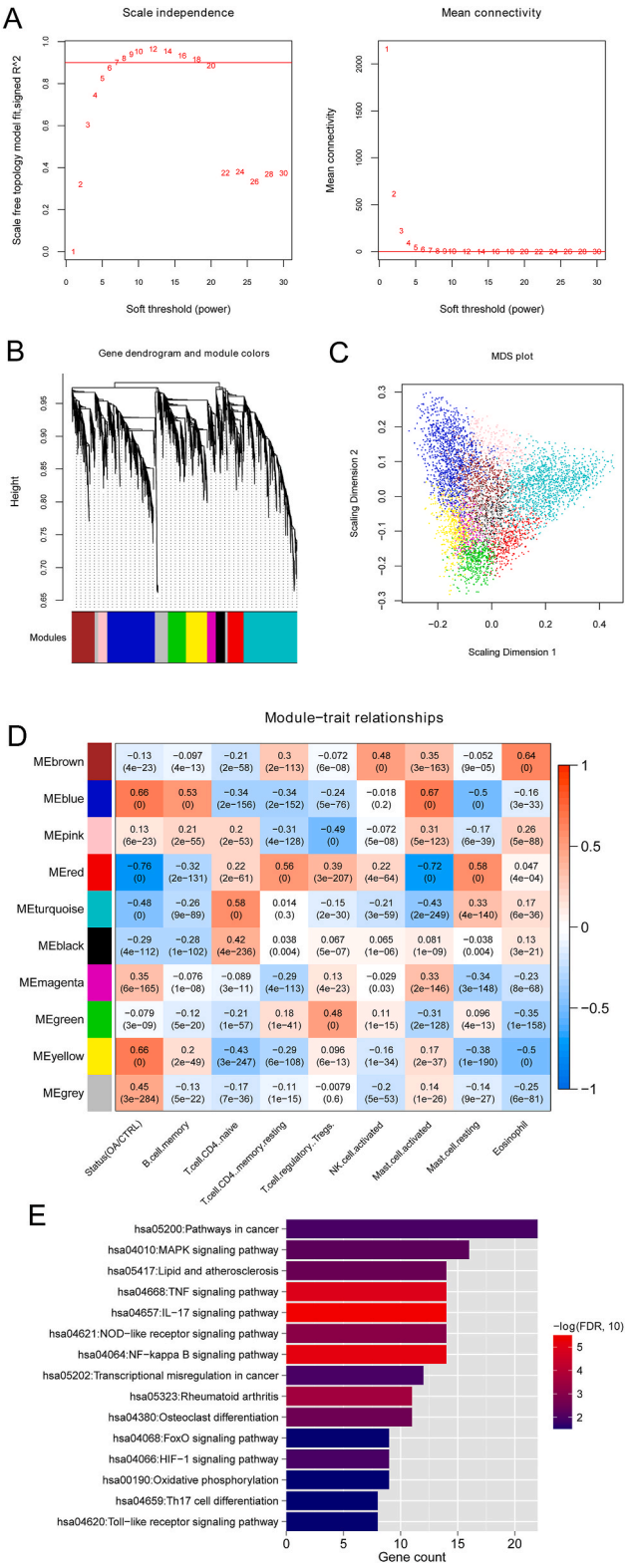

Fig. 5. Screening of modules related to disease progression and immunity. A: Left: The selection process for the adjacency matrix weight parameter power. The red line signifies the standard line where the squared value of the correlation coefficient reaches 0.9. On the right, the average connectivity of genes is displayed under different power parameters. B: The tree diagram visually presents the division of modules, with each color representing a distinct module. C: The MDS diagram showcases the genes contained within each module. D: A heatmap demonstrates the correlation

between the proportion of immune cells in the sample and the modules obtained through partitioning. E: The enriched GO functions and KEGG signaling pathways attributed to module genes. (For interpretation of the references to color in this figure legend, the reader is referred to the Web version of this article.)

Table 3
Modules identified from WGCNA.

ID	Color	Module size	#DEGs	Enrichment infor	
				Enrichment fold[95%CI]	P_{hyper}
module 1	black	234	1	0.0759 [0.00191–0.430]	1.08E-04
module 2	blue	1193	112	1.667 [1.319–2.094]	1.72E-05
module 3	brown	571	22	0.684 [0.419–1.065]	9.82E-02
module 4	green	450	–	–	–
module 5	grey	485	1	0.0367 [0.000927–0.206]	3.14E-10
module 6	magenta	215	2	0.165 [0.0198–0.609]	1.47E-03
module 7	pink	229	–	–	–
module 8	red	401	63	2.789 [2.055–3.742]	2.43E-10
module 9	turquoise	1321	97	1.304 [1.019–1.656]	2.91E-02
module 10	yellow	531	19	0.636 [0.374–1.019]	5.61E-02

Table 4
The KEGG enrichment of 65 immune-related genes.

Term	Count	FDR	Genes
hsa04657:IL-17 signaling pathway	14	3.65E-06	JUN, HSP90AA1, CEBPB, JUND, CXCL8, TNFAIP3, CXCL1, FOS, CXCL3, CXCL2, NFKBIA, IL6, IL1B, FOSB
hsa04064:NF-kappa B signaling pathway	14	6.31E-06	CXCL8, GADD45B, IL1R1, TNFAIP3, CXCL1, CXCL3, CXCL2, NFKB2, ICAM1, NFKBIA, PLAU, IL1B, CCL4, CCL19
hsa04668:TNF signaling pathway	14	1.03E-05	JUN, CEBPB, TNFAIP3, CXCL1, FOS, CXCL3, CXCL2, ICAM1, NFKBIA, SOCS3, IL6, IL1B, IRF1, JUNB
hsa05323:Rheumatoid arthritis	11	2.62E-04	IL6, ATP6V0B, JUN, CXCL8, IL1B, CCL3, CXCL1, FOS, CXCL3, CXCL2, ICAM1
hsa04621:NOD-like receptor signaling pathway	14	9.18E-04	GABARAPL2, JUN, HSP90AA1, GABARAPL1, CXCL8, TNFAIP3, CXCL1, CYBA, CXCL3, CXCL2, NFKBIA, IL6, IL1B, TRIP6
hsa04380:Osteoclast differentiation	11	2.68E-03	NFKBIA, SOCS3, JUN, JUND, IL1R1, IL1B, FOSB, CYBA, FOS, JUNB, NFKB2
hsa05417:Lipid and atherosclerosis	14	3.38E-03	JUN, HSP90AA1, CXCL8, CXCL1, CYBA, FOS, CXCL3, CXCL2, ICAM1, NFKBIA, IL6, IL1B, CCL3, HSPA1B
hsa04010:MAPK signaling pathway	16	5.95E-03	DUSP5, JUN, JUND, GADD45B, IL1R1, DUSP1, PDGFA, FOS, EGFR, NFKB2, NR4A1, MYC, IL1B, PDGFC, MAPKAPK2, HSPA1B
hsa05200:Pathways in cancer	22	1.14E-02	CEBPA, CDKN1A, JUN, HSP90AA1, CXCL8, GADD45B, MGST3, PDGFA, FOS, HIF1A, EGFR, NFKB2, RBX1, NFKBIA, BMP2, IL6, GSTA4, LPAR6, MYC, PIM1, HMOX1, ELOB
hsa05202:Transcriptional misregulation in cancer	12	1.18E-02	CEBPA, IL6, CDKN1A, DDX5, CEBPB, CXCL8, GADD45B, BCL6, PLAU, MYC, ID2, PDGFA
hsa04066:HIF-1 signaling pathway	9	1.18E-02	IL6, CDKN1A, PFKFB3, TFRC, HMOX1, ELOB, HIF1A, EGFR, RBX1
hsa04068:FoxO signaling pathway	9	2.99E-02	GABARAPL2, IL6, CDKN1A, GABARAPL1, GADD45B, BCL6, SGK1, EGFR, KLF2
hsa04620:Toll-like receptor signaling pathway	8	3.02E-02	NFKBIA, IL6, JUN, CXCL8, IL1B, CCL4, CCL3, FOS
hsa00190:Oxidative phosphorylation	9	3.16E-02	NDUFA8, ATP6V0B, NDUFA13, NDUFB5, NDUFA3, NDUFS4, NDUFS3, UQCR10, COX5B
hsa04659:Th17 cell differentiation	8	3.35E-02	NFKBIA, IL6, HSP90AA1, JUN, IL1R1, IL1B, FOS, HIF1A

Note: FDR, false discovery rate.

validation datasets. The nomogram model models have proven to be effective in predicting individual disease risk or prognosis across various diseases. In OA, Zhang et al. developed a nomogram model that pulse, age, mean corpuscular hemoglobin concentration, absolute value of lymphocytes, and blood urea nitrogen to predict the severity of knee OA without relying on imaging techniques [42]. There are also studies developed nomogram models with 3D gait analysis system or MRI parameters for predicting knee instability in OA patients [43–45]. In recent years, more studies focused on developing nomogram model with key genes participating in the development of OA [46–49]. Li et al. developed a nomogram model for diagnosing OA with metabolic syndrome with immune-associated genes. These nomogram models, together with ours, might be promising in accurately diagnosing OA patients.

In addition to immune cells, some inflammatory pathways and genes were also identified. *CEBPB*, *CXCL1* and *JUND* were found to be involved in TNF signaling pathway and IL-17 signaling pathway. *CEBPB* is one of the strongest *trans*-activators in chondrocytes, and plays a key role in endochondral osteogenesis [50]. *CXCL1* is a key chemoattractant for neutrophils [51], which can induce

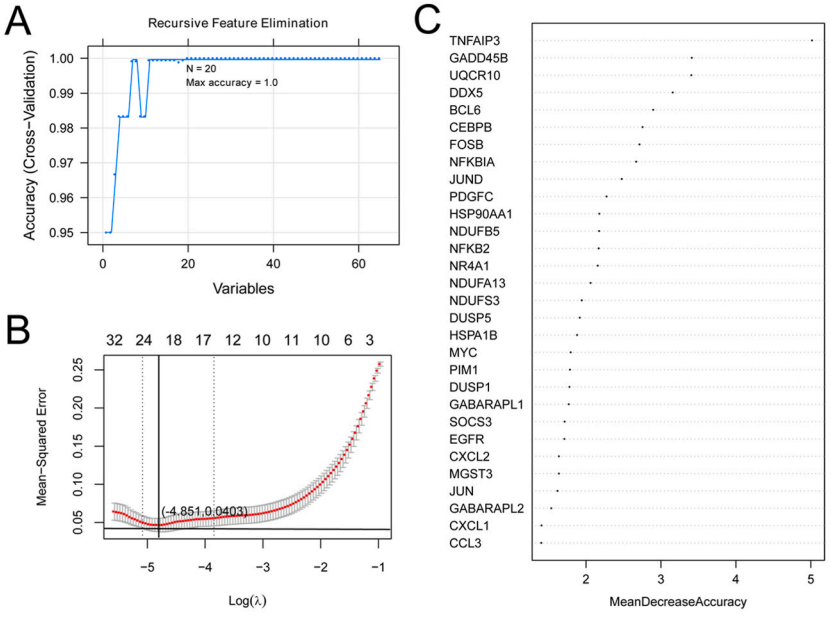

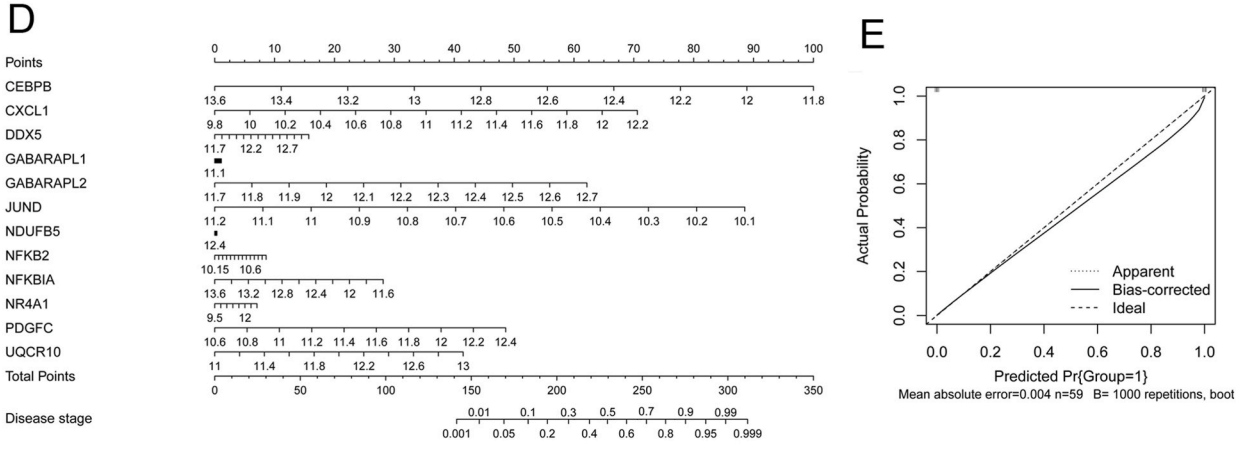

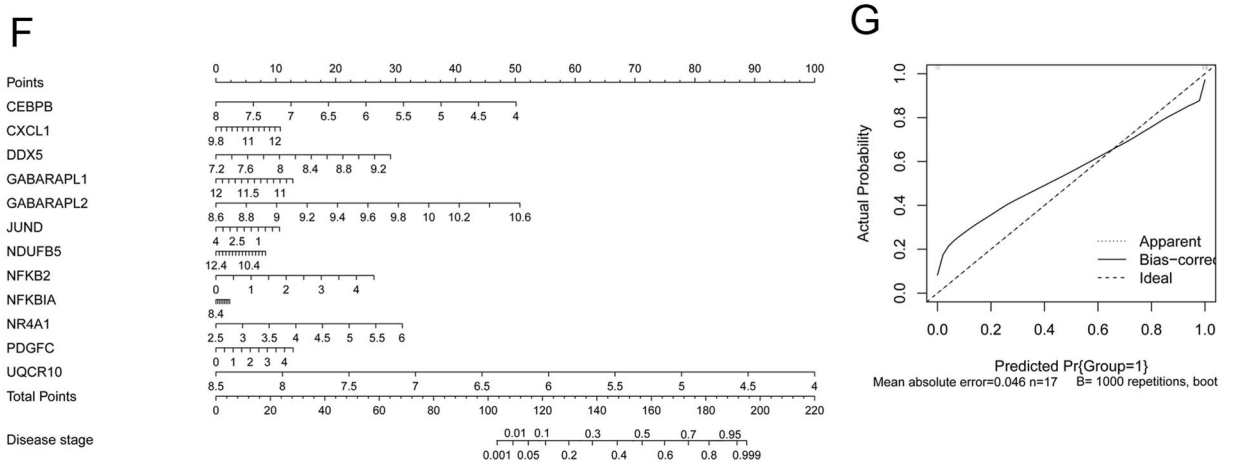

(caption on next page)

Fig. 6. Construction and verification of a Nomogram diagnostic model. A–C: Parameter diagram of feature gene screening based on (A) LASSO, (B) RFE and (C) RF algorithms. D: Nomogram model based on the expression levels of 12 feature genes in the combined training dataset. E: The calibration curves of Nomogram model of the combined training dataset. The horizontal and vertical axes represented the calculated and actual probabilities, respectively. The solid line depicted the performance of an ideal diagnostic model, while the dotted line illustrated the performance of the developed nomogram model. F: Nomogram model based on the expression levels of 12 feature genes in the validation dataset. G: The calibration curves of Nomogram of the validation dataset.

chondrocyte apoptosis during cartilage development [52]. JUND is a transcription factor, which can transcriptionally activate lncRNA LOXL1-AS1 and promote the progression of osteoarthritis [53]. IL-17 and its upstream regulatory factor IL-23 have been reported to promote the secretion of inflammatory factors and can increase the pathological progress of OA [54]. TNF-α, as a proinflammatory cytokine, assumes a central role in the pathogenesis of osteoarthritis by amplifying the activity of proteolytic enzymes [55]. For the other two validated genes, GABARAPL2 was enriched in FoxO signaling pathway. FoxOs are important regulators of bone resorption and osteoclast differentiation [56]. A recent study has reported that the FoxO signaling pathway exhibits significant dysregulation in human OA cartilage when compared to normal tissues [57]. Wu et al. [58] reported that GABARAP may augment the protection effect of differentiated chondrocytes by inducing autophagy and reducing the anti-inflammatory pathway, thereby slowing OA progression [58]. *PDGFC* was enriched in MAPK signaling pathway. Platelet-derived growth factors have been shown to play a significant role in synovial hyperplasia [59]. Pohlers et al. [60] provided evidence demonstrating the expression of PDGFC by synovial fibroblasts and macrophages in the synovial membrane of patients with OA. MAPK signaling has been well recognized to involve in the progression of OA and may serve as effective treatment targets of OA [61]. Overall, these genes may serve as biomarkers of OA.

Furthermore, based on the 12 feature immune DEGs, small molecular chemical drugs that were directly related to OA were extracted, such as acetaminophen, aspirin, and caffeine. Acetaminophen could affect the expression of CEBPB, DDX5, GABARAPL1 and NFKBIA, increase the expression of CXCL1, GABARAPL2, JUND, NFKB2 and NR4A1, and decrease the expression of NDUFB5 and PDGFC. Paracetamol (acetaminophen) is an effective agent to relieve pain of OA and is recommended for analgesia at an early stage during treating OA 63, 64. Aspirin could promote the reaction of CEBPB binding to IL4 promoter polymorphism, increase the secretion of CXCL1, increase the expression of DDX5 and NFKBIA, and decrease the expression of JUND. Aspirin is associated with reduced cartilage loss in knee osteoarthritis [62]. Caffeine could decrease the expression of CEBPB and NDUFB5 and increase phosphorylation of NFKBIA. Caffeine is a natural alkaloid of the methylxantines family, which has detrimental effects on both articular and growth plate hyaline cartilage. Therefore, moderating caffeine consumption may be important for patients with OA, although the association between caffeine and OA remains a topic of debate.

There are some limitations in our study. First, the key genes were only validated in synovial membrane of OA rats by qRT-PCR and the histological images of the rats with synovial membrane inflammation/fibrosis were not evaluated. Second, though small molecule chemical drugs related with OA were identified, their effects were not investigated in *in vitro* or *in vivo* studies. Third, the diagnostic model should be further validated in clinical trials. Therefore, this study is a preliminary study and further studies are still warranted in future.

5. Conclusion

In conclusion, a diagnostic model utilizing twelve immune-related genes was bulit. These model genes, such as *CEBPB*, *CXCL1*, GABARAPL2, and *PDGFC*, may serve as diagnostic biomarkers and immunotherapeutic targets.

Ethics approval and consent to participate

This study was supported by the Experimental Animal Ethics Committee of Shanghai Ninth People's Hospital, Shanghai Jiao Tong University School of Medicine (special for project application) (Approval number: SH9H-2022-A115-SB). All methods were carried out in accordance with relevant guidelines and regulations and are reported in accordance with ARRIVE guidelines (https://arriveguidelines.org) for the reporting of animal experiments.

Consent for publication

Not applicable.

Data Availability Statement

Data will be made available on request.

Funding

This work was supported by Stroke Screening and Prevention Project Committee, National Health and Family Planning Commission, P.R.China (No. GN-2018R0010), Northern Jiangsu People's Hospital (No. DTRB18005), General project of Jiangsu Provincial Health Commission (NO. H2023006), the Natural Science Foundation of Shanghai (No. 22ZR1437600), and the Science and

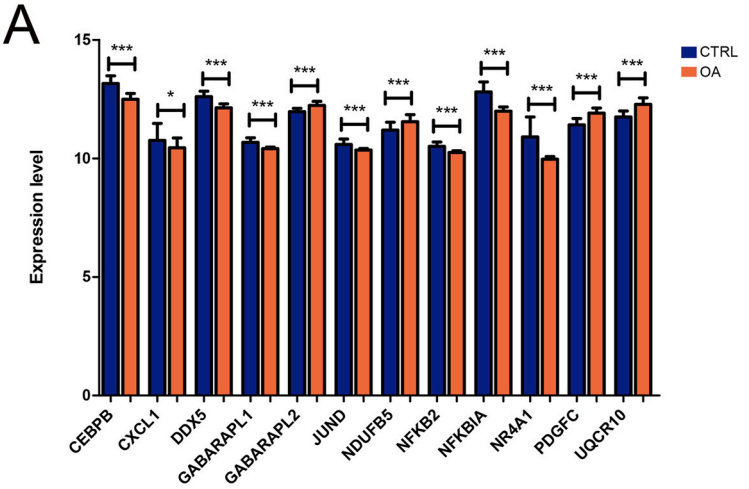

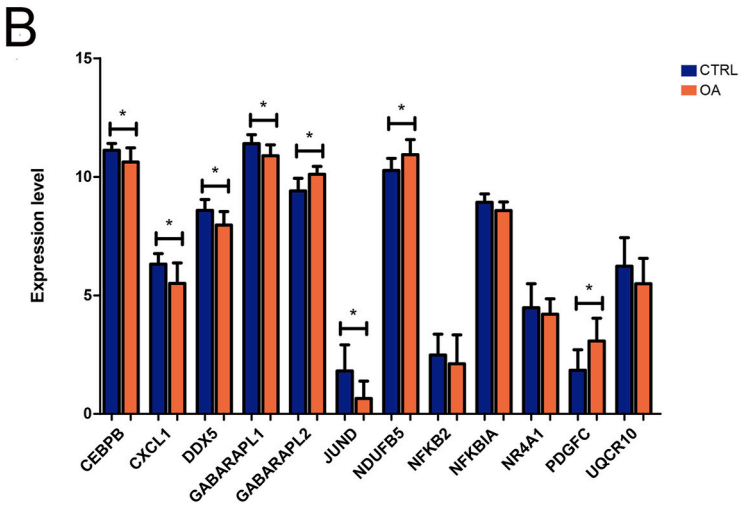

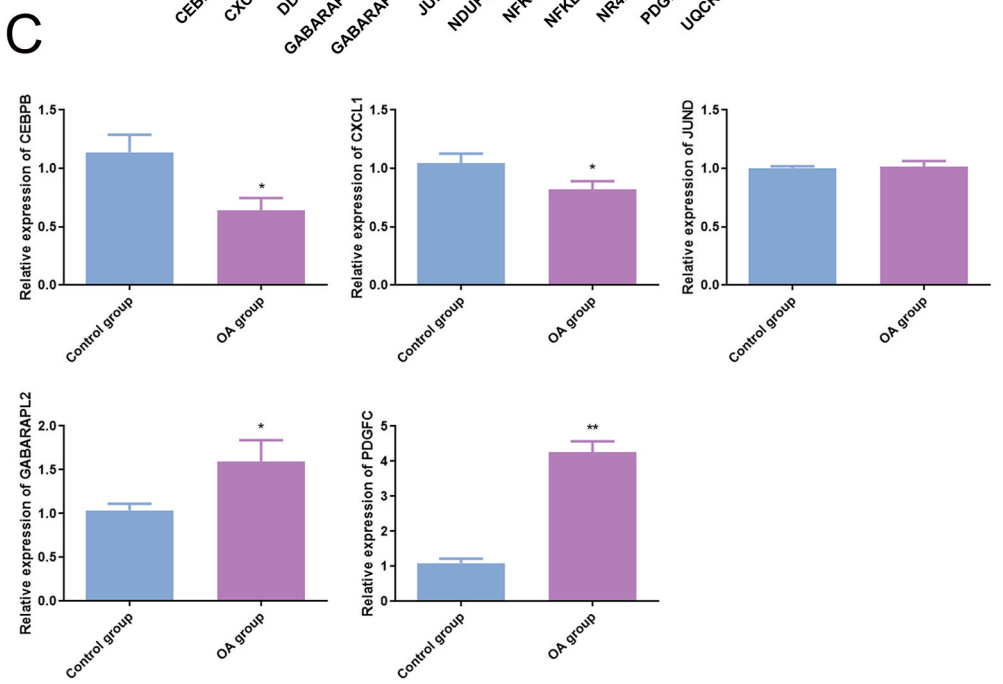

(caption on next page)

Fig. 7. Verification of key genes in the nomogram model. The expression levels of 12 genes in the training dataset (A) and GSE82107 validation dataset (B). (C) The expression levels of *CEBPB*, *CXCL1*, *JUND*, GABARAPL2 and *PDGFC* in OA group compared with control detected by qRT-PCR. *P < 0.05, **P < 0.01, ***P < 0.001.

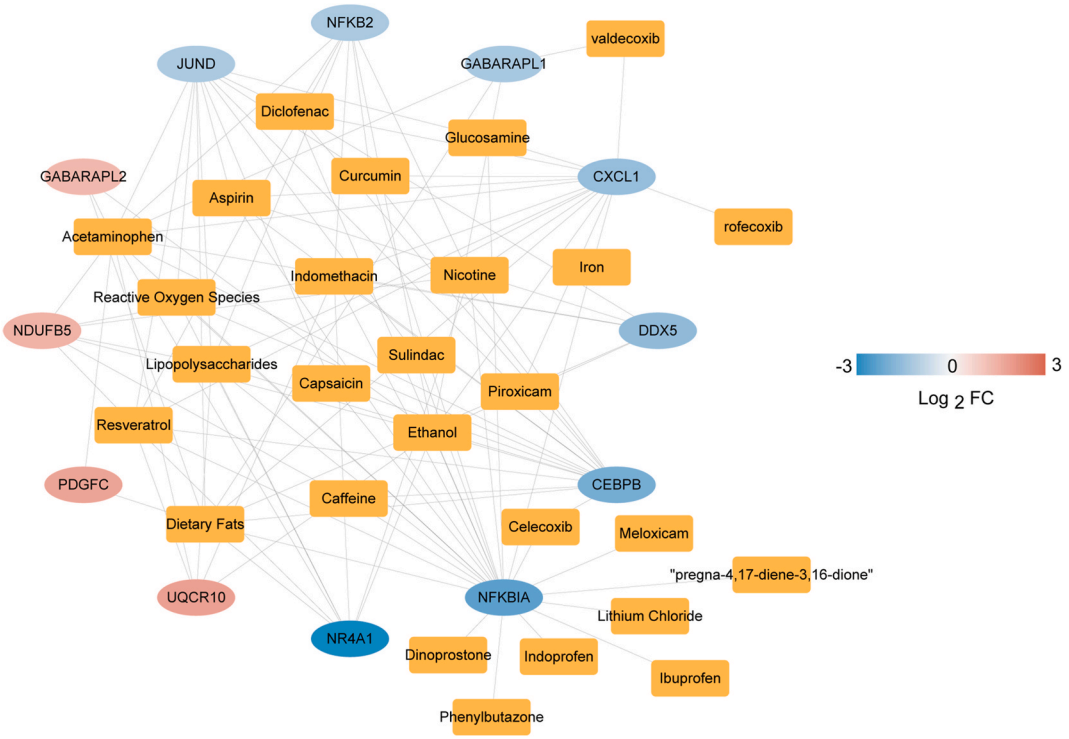

Fig. 8. The network of the 12 feature immune-related genes and small molecular chemical drugs.

Technology Committee of Fengxian District, Shanghai (No. FK20201501).

CRediT authorship contribution statement

Bo Chen: Writing – original draft, Methodology, Conceptualization. **Chun Lin:** Writing – original draft, Methodology, Conceptualization. **Xing Jin:** Investigation, Data curation. **Xibin Zhang:** Investigation, Data curation. **Kang Yang:** Investigation, Data curation. **Jianjian Wang:** Software, Formal analysis. **Feng Zhang:** Software, Formal analysis. **Yuxin Zhang:** Software, Formal analysis. **Yingying Ji:** Validation, Formal analysis. **Zhaoxiang Meng:** Writing – review & editing, Validation, Formal analysis.

Declaration of competing interest

The authors declare that they have no known competing financial interests or personal relationships that could have appeared to influence the work reported in this paper.

Acknowledgements

None.

Appendix A. Supplementary data

Supplementary data to this article can be found online at https://doi.org/10.1016/j.heliyon.2023.e23636.

List of abbreviations

OA	osteoarthritis
DEGs	differentially expressed genes

PCC	Pearson correlation coefficient
BP	biological process
DC	degree centrality
CC	closeness centrality
BC	betweenness centrality
Tregs	T cell regulatory

References

[1] D. Chen, J. Shen, W. Zhao, T. Wang, L. Han, J.L. Hamilton, et al., Osteoarthritis: toward a comprehensive understanding of pathological mechanism, Bone research 5 (2017) 1–13.
[2] C.A. Murphy, A.K. Garg, J. Silva-Correia, R.L. Reis, J.M. Oliveira, M.N. Collins, The meniscus in normal and osteoarthritic tissues: facing the structure property challenges and current treatment trends, Annu. Rev. Biomed. Eng. 21 (2019) 495–521.
[3] N. Zeng, Z.P. Yan, X.Y. Chen, G.X. Ni, Infrapatellar fat pad and knee osteoarthritis, Aging Dis 11 (2020) 1317–1328.
[4] J. Martel-Pelletier, A.J. Barr, F.M. Cicuttini, P.G. Conaghan, C. Cooper, M.B. Goldring, et al., Osteoarthritis, Nat Rev Dis Primers 2 (2016), 16072.
[5] M. Cross, E. Smith, D. Hoy, S. Nolte, I. Ackerman, M. Fransen, et al., The global burden of hip and knee osteoarthritis: estimates from the global burden of disease 2010 study, Annals of the rheumatic diseases 73 (2014) 1323–1330.
[6] J.G. Quicke, P.G. Conaghan, N. Corp, G. Peat, Osteoarthritis year in review 2021: epidemiology & therapy, Osteoarthritis Cartilage 30 (2022) 196–206.
[7] Q. Yao, X. Wu, C. Tao, W. Gong, M. Chen, M. Qu, et al., Osteoarthritis: pathogenic signaling pathways and therapeutic targets, Signal Transduct Target Ther 8 (2023) 56.
[8] B.E. Elsadek, A.A. Abdelghany, M.A. Abd EL-Aziz, H.R. Madkor, A. Abd Elrady Ahmed, S.K. Abd-Elghaffar, et al., Validation of the diagnostic and prognostic values of ADAMTS5 and FSTL1 in osteoarthritis rat model, Cartilage 13 (2021) 1263S–1273S.
[9] I. Atukorala, C.K. Kwoh, A. Guermazi, F.W. Roemer, R.M. Boudreau, M.J. Hannon, et al., Synovitis in knee osteoarthritis: a precursor of disease? Ann. Rheum. Dis. 75 (2016) 390–395.
[10] F. Eymard, A. Pigenet, D. Citadelle, C.H. Flouzat-Lachaniette, A. Poignard, C. Benelli, et al., Induction of an inflammatory and prodegradative phenotype in autologous fibroblast-like synoviocytes by the infrapatellar fat pad from patients with knee osteoarthritis, Arthritis Rheumatol. 66 (2014) 2165–2174.
[11] V. Macchi, E. Stocco, C. Stecco, E. Belluzzi, M. Favero, A. Porzionato, et al., The infrapatellar fat pad and the synovial membrane: an anatomo-functional unit, J. Anat. 233 (2018) 146–154.
[12] E. Kalaitzoglou, T.M. Griffin, M.B. Humphrey, Innate immune responses and osteoarthritis, Curr. Rheumatol. Rep. 19 (2017) 1–6.
[13] N. Fahy, E. Farrell, T. Ritter, A.E. Ryan, J.M. Murphy, Immune modulation to improve tissue engineering outcomes for cartilage repair in the osteoarthritic joint, Tissue Engineering Part B: Reviews 21 (2015) 55–66.
[14] X. Ayral, E. Pickering, T. Woodworth, N. Mackillop, M. Dougados, Synovitis: a potential predictive factor of structural progression of medial tibiofemoral knee osteoarthritis–results of a 1 year longitudinal arthroscopic study in 422 patients, Osteoarthritis Cartilage 13 (2005) 361–367.
[15] C.R. Scanzello, B. McKeon, B.H. Swaim, E. DiCarlo, E.U. Asomugha, V. Kanda, et al., Synovial inflammation in patients undergoing arthroscopic meniscectomy: molecular characterization and relationship to symptoms, Arthritis Rheum. 63 (2011) 391–400.
[16] E. Olivotto, G. Trisolino, E. Belluzzi, A. Lazzaro, A. Strazzari, A. Pozzuoli, et al., Macroscopic synovial inflammation Correlates with symptoms and cartilage Lesions in patients undergoing arthroscopic partial meniscectomy: a clinical study, J. Clin. Med. (2022) 11.
[17] H. Jasin, Immune mediated cartilage destruction, Scand. J. Rheumatol. 17 (1988) 111–116.
[18] C. Bonnet, D. Walsh, Osteoarthritis, angiogenesis and inflammation, Rheumatology 44 (2005) 7–16.
[19] B. Moradi, N. Rosshirt, E. Tripel, J. Kirsch, A. Barie, F. Zeifang, et al., Unicompartmental and bicompartmental knee osteoarthritis show different patterns of mononuclear cell infiltration and cytokine release in the affected joints, Clin. Exp. Immunol. 180 (2015) 143–154.
[20] J.T. Leek, W.E. Johnson, H.S. Parker, A.E. Jaffe, J.D. Storey, The sva package for removing batch effects and other unwanted variation in high-throughput experiments, Bioinformatics 28 (2012) 882–883.
[21] M.E. Ritchie, B. Phipson, D. Wu, Y. Hu, C.W. Law, W. Shi, et al., Limma powers differential expression analyses for RNA-sequencing and microarray studies, Nucleic acids research 43 (2015) e47.
[22] L. Wang, C. Cao, Q. Ma, Q. Zeng, H. Wang, Z. Cheng, et al., RNA-seq analyses of multiple meristems of soybean: novel and alternative transcripts, evolutionary and functional implications, BMC Plant Biol. 14 (2014) 169.
[23] W. Press, S. Teukolsky, W. Vetterling, B. Flannery, Section 16.4. Hierarchical Clustering by Phylogenetic Trees. *Numerical Recipes: the Art of Scientific Computing*, 2007, pp. 868–881.
[24] M.M. Deza, E. Deza, Encyclopedia of distances, in: Encyclopedia of Distances, edn., Springer, 2009, pp. 1–583.
[25] B. Chen, M.S. Khodadoust, C.L. Liu, A.M. Newman, A.A. Alizadeh, Profiling tumor infiltrating immune cells with CIBERSORT, in: Cancer Systems Biology, edn., Springer, 2018, pp. 243–259.
[26] D.W. Huang, B.T. Sherman, R.A. Lempicki, Systematic and integrative analysis of large gene lists using DAVID bioinformatics resources, Nat. Protoc. 4 (2009) 44–57.
[27] D.W. Huang, B.T. Sherman, R.A. Lempicki, Bioinformatics enrichment tools: paths toward the comprehensive functional analysis of large gene lists, Nucleic acids research 37 (2009) 1–13.
[28] D. Szklarczyk, A.L. Gable, K.C. Nastou, D. Lyon, R. Kirsch, S. Pyysalo, et al., The STRING database in 2021: customizable protein–protein networks, and functional characterization of user-uploaded gene/measurement sets, Nucleic acids research 49 (2021) D605–D612.
[29] P. Shannon, A. Markiel, O. Ozier, N.S. Baliga, J.T. Wang, D. Ramage, et al., Cytoscape: a software environment for integrated models of biomolecular interaction networks, Genome Res. 13 (2003) 2498–2504.
[30] G. Scardoni, M. Petterlini, C. Laudanna, Analyzing biological network parameters with CentiScaPe, Bioinformatics 25 (2009) 2857–2859.
[31] P. Langfelder, S. Horvath, WGCNA: an R package for weighted correlation network analysis, BMC Bioinf. 9 (2008) 1–13.
[32] T.M. Deist, F.J. Dankers, G. Valdes, R. Wijsman, I.C. Hsu, C. Oberije, et al., Machine learning algorithms for outcome prediction in (chemo) radiotherapy: an empirical comparison of classifiers, Medical physics 45 (2018) 3449–3459.
[33] J.J. Goeman, L1 penalized estimation in the Cox proportional hazards model, Biom. J. 52 (2010) 70–84.
[34] L. Tolo̧si, T. Lengauer, Classification with correlated features: unreliability of feature ranking and solutions, Bioinformatics 27 (2011) 1986–1994.
[35] J. Wu, H. Zhang, L. Li, M. Hu, L. Chen, B. Xu, et al., A nomogram for predicting overall survival in patients with low-grade endometrial stromal sarcoma: a population-based analysis, Cancer Commun. 40 (2020) 301–312.
[36] F.E. Harrell Jr., K.L. Lee, D.B. Mark, Multivariable prognostic models: issues in developing models, evaluating assumptions and adequacy, and measuring and reducing errors, Stat. Med. 15 (1996) 361–387.
[37] J.E. Woodell-May, S.D. Sommerfeld, Role of inflammation and the immune system in the progression of osteoarthritis, Journal of Orthopaedic Research® 38 (2020) 253–257.
[38] N. Rosshirt, S. Hagmann, E. Tripel, T. Gotterbarm, J. Kirsch, F. Zeifang, et al., A predominant Th1 polarization is present in synovial fluid of end-stage osteoarthritic knee joints: analysis of peripheral blood, synovial fluid and synovial membrane, Clin. Exp. Immunol. 195 (2019) 395–406.

[39] R.-R. Da, Y. Qin, D. Baeten, Y. Zhang, B cell clonal expansion and somatic hypermutation of Ig variable heavy chain genes in the synovial membrane of patients with osteoarthritis, J. Immunol. 178 (2007) 557–565.
[40] S.C. Bischoff, Role of mast cells in allergic and non-allergic immune responses: comparison of human and murine data, Nat. Rev. Immunol. 7 (2007) 93–104.
[41] B.J. de Lange-Brokaar, M. Kloppenburg, S. Andersen, A. Dorjée, E. Yusuf, L. Herb-van Toorn, et al., Characterization of synovial mast cells in knee osteoarthritis: association with clinical parameters, Osteoarthritis Cartilage 24 (2016) 664–671.
[42] Q. Zhang, Y. Yao, J. Wang, Y. Chen, D. Ren, P. Wang, A Simple nomogram for predicting osteoarthritis severity in patients with knee osteoarthritis, Comput. Math. Methods Med. 2022 (2022), 3605369.
[43] C. Gu, Y. Mao, H. Dong, Y. Cui, M. Fu, Nomogram in knee instability: 3D gait analysis of knee osteoarthritis patients, Indian J. Orthop. 56 (2022) 1554–1564.
[44] Y. Sun, C. Deng, Z. Zhang, X. Ma, F. Zhou, X. Liu, Novel nomogram for predicting the progression of osteoarthritis based on 3D-MRI bone shape: data from the FNIH OA biomarkers consortium, BMC Musculoskelet Disord 22 (2021) 782.
[45] Z. Shao, Z. Liang, P. Hu, S. Bi, A nomogram based on radiological features of MRI for predicting the risk of severe pain in patients with osteoarthritis of the knee, Front Surg 10 (2023), 1030164.
[46] W. Wang, Z. Chen, Y. Hua, Bioinformatics prediction and experimental validation identify a novel Cuproptosis-related gene signature in human synovial inflammation during osteoarthritis progression, Biomolecules 13 (2023).
[47] Y. Duan, C. Yu, M. Yan, Y. Ouyang, S. Ni, m6A regulator-mediated RNA methylation modification patterns regulate the immune microenvironment in osteoarthritis, Front. Genet. 13 (2022), 921256.
[48] S. Hu, C. Shen, X. Yao, Y. Zou, T. Wang, X. Sun, et al., m6A regulator-mediated methylation modification patterns and immune microenvironment infiltration characterization in osteoarthritis, BMC Med Genomics 15 (2022) 273.
[49] Z. Chen, W. Wang, Y. Zhang, X. Xue, Y. Hua, Identification of four-gene signature to diagnose osteoarthritis through bioinformatics and machine learning methods, Cytokine 169 (2023), 156300.
[50] M. Hirata, F. Kugimiya, A. Fukai, S. Ohba, N. Kawamura, T. Ogasawara, et al., C/EBPβ promotes transition from proliferation to hypertrophic differentiation of chondrocytes through transactivation of p57Kip2, PLoS One 4 (2009) e4543.
[51] K.V. Sawant, K.M. Poluri, A.K. Dutta, K.M. Sepuru, A. Troshkina, R.P. Garofalo, et al., Chemokine CXCL1 mediated neutrophil recruitment: role of glycosaminoglycan interactions, Sci. Rep. 6 (2016).
[52] E. Olivotto, R. Vitellozzi, P. Fernandez, E. Falcieri, M. Battistelli, S. Burattini, et al., Chondrocyte hypertrophy and apoptosis induced by GROα require three-dimensional interaction with the extracellular matrix and a co-receptor role of chondroitin sulfate and are associated with the mitochondrial splicing variant of cathepsin B, J. Cell. Physiol. 210 (2007) 417–427.
[53] K. Chen, H. Fang, N. Xu, LncRNA LOXL1-AS1 is transcriptionally activated by JUND and contributes to osteoarthritis progression via targeting the miR-423-5p/KDM5C axis, Life Sci. 258 (2020), 118095.
[54] A. Askari, M.M. Naghizadeh, R. Homayounfar, A. Shahi, M.H. Afsarian, A. Paknahad, et al., Increased serum levels of IL-17A and IL-23 are associated with decreased vitamin D3 and increased pain in osteoarthritis, PLoS One 11 (2016), e0164757.
[55] C.-H. Su, C.-Y. Lin, C.-H. Tsai, H.-P. Lee, L.-C. Lo, W.-C. Huang, et al., Betulin suppresses TNF-α and IL-1β production in osteoarthritis synovial fibroblasts by inhibiting the MEK/ERK/NF-κB pathway, J. Funct.Foods 86 (2021), 104729.
[56] S.M. Bartell, H.-N. Kim, E. Ambrogini, L. Han, S. Iyer, S. Serra Ucer, et al., FoxO proteins restrain osteoclastogenesis and bone resorption by attenuating H2O2 accumulation, Nat. Commun. 5 (2014) 1–12.
[57] K.M. Fisch, R. Gamini, O. Alvarez-Garcia, R. Akagi, M. Saito, Y. Muramatsu, et al., Identification of transcription factors responsible for dysregulated networks in human osteoarthritis cartilage by global gene expression analysis, Osteoarthritis Cartilage 26 (2018) 1531–1538.
[58] Z. Wu, H. Lu, J. Yao, X. Zhang, Y. Huang, S. Ma, et al., Retracted: GABARAP promotes bone marrow mesenchymal stem cells-based the osteoarthritis cartilage regeneration through the inhibition of PI3K/AKT/mTOR signaling pathway, J. Cell. Physiol. 234 (2019) 21014–21026.
[59] K. Rubin, L. Terracio, L. Rönnstrand, C.H. Heldin, L. Klareskog, Expression of platelet-derived growth factor receptors is induced on connective tissue cells during chronic synovial inflammation, Scand. J. Immunol. 27 (1988) 285–294.
[60] D. Pohlers, R. Huber, B. Ukena, R.W. Kinne, Expression of platelet-derived growth factors C and D in the synovial membrane of patients with rheumatoid arthritis and osteoarthritis, Arthritis Rheum. 54 (2006) 788–794.
[61] J. Ran, C. Ma, K. Xu, L. Xu, Y. He, S.A.A. Moqbel, et al., Schisandrin B ameliorated chondrocytes inflammation and osteoarthritis via suppression of NF-κB and MAPK signal pathways, Drug Des. Dev. Ther. 12 (2018) 1195–1204.
[62] A.E. Wluka, C. Ding, Y. Wang, G. Jones, D.M. Urquhart, F.M. Cicuttini, Aspirin is associated with reduced cartilage loss in knee osteoarthritis: data from a cohort study, Maturitas 81 (2015) 394–397.